TECHNICAL RESEARCH REPORT

Hardness Assessment of Human Enamel

by G. Zhang, S.J. Ng, D.T. Le, D. Young

T.R. 97-42

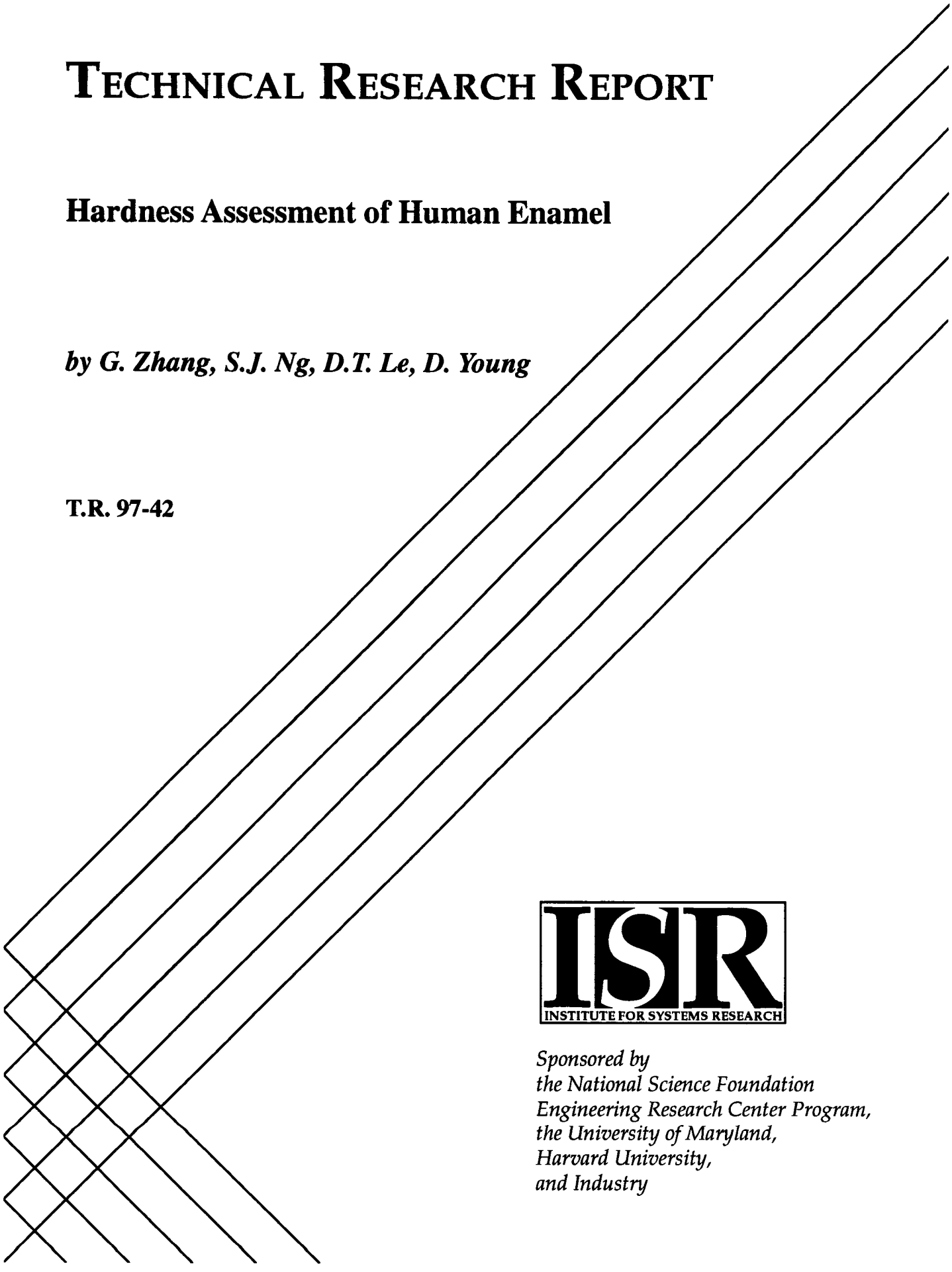

Sponsored by
the National Science Foundation
Engineering Research Center Program,
the University of Maryland,
Harvard University,
and Industry

HARDNESS ASSESSMENT OF HUMAN ENAMEL

Guangming Zhang, Stanley J. Ng, Dung T. Le, and Daniel Young
Department of Mechanical Engineering & the Institute for Systems Research
University of Maryland
College Park, Maryland 20742

Abstract

This paper presents results from investigating indentation impressions on human enamel under micro-hardness tests. The experiments of hardness testing were performed on a microhardness indentation machine under different loading conditions. Images of indentation impressions were obtained using an environmental scanning electron microscope. Geometrical shapes of hardness indentations were visualized in three-dimensional space using computer graphics. Quantitative information was obtained through atomic force measurements to characterize "pile-up", "sink-in", and elastic recovery of enamel. Special efforts have been made to study the microstrucutual effect of the calcified rods orientations on the fracture patterns formed during the hardness tests. Significant findings include that the occlusal surface demonstrates much stronger resistance to the indentation force than does the buccal surface and shows 40% elastic recovery after indentation. A new formula to determine hardness value has been proposed. By incorporating the reversible deformation into the evluation, a normalized hardness measurement can be made to form a basis for comparison and other investigations where hardness has its unique role to play.

1. Introduction

Advanced ceramic materials have been successfully developed during the past decades. They are widely used in a variety of applications for their superior properties, such as high-strength-to-mass ratio, excellent wear resistance and exceptional corrosion resistance, compared to conventional materials, such as metals and plastics. The capability of ceramics to be manufactured to near net shape by pressing and sintering processes also makes economic production of ceramics possible. These intrinsic properties and advances in manufacturing technology have led ceramics to be prime candidates for dental restorative fabrications [1-2].

As new types of ceramic material merge, assessment of their machinability becomes critical to ensure dental restorations made from them meet clinic requirements and patient needs. The research work presented in this paper is on microhardness tests of human enamel. The obtained information will be used as a critical reference to assess the

feasibility of new ceramic materials for use as dental restorative materials. Behavior of material under the hardness testing in general reflects the characteristics of the material removal during machining [1-4]. Therefore, results from the microhardness testing can be directly used to assess their machinability. It should be noted that scientific research in the study of the structure of human enamel has been carried out for decades. Significant progress has been made to understand the structure and function of human enamel [5-6]. The methodology developed in this research is new and different from those previously used in the dental research. It combines recently developed image processing technology, computer graphics, and fracture mechanics. Advanced measurement techniques, such as environmental scanning electron microscope and atomic force microscope, are used to provide quantitative information. The objective of this study is to investigate the behaviour of enamel material under hardness testing with emphasis on the effect of enamel rod orientation on the hardness. Such information for newly developed ceramic materials should be valuable assessment as it relates to material removal during shaping of dental restorations.

2. Specimen Preparation and Hardness Testing

As stated, a special objective of this research is to study the microstructural effect of the enamel rod orientations on the hardness measurement. In order to determine the effect of rod orientation, two different planes on the tooth are used for indentation. As illustrated in Figure 1, a tooth is first set in an orientation such that the buccal or occlusal surface is parallel to the testing surface. When the occlusal surface is tested, the enamel rods are aligned with the indentation loading. On the other hand, when the buccal surface is tested, the enamel rods are oriented at an angle to the indentation loading. Acrylic resin is used to mount the tooth in this orientation [8]. The exposed surfaces are polished using a set of grit-sized papers and finally with diamond paste. The polishing sequence results in an enamel surface within a 1/4 micron surface roughness.

Specimens prepared in the two different orientations are tested on a Microhardness Indentation Tester Model 300 [9]. A Vicker's indentor which is a pyramid with edge angle of 136° is used. Eight loading conditions used vary from 50 grams to 2000 grams to model normal funtional forces [10]. Under each loading condition, two hardness indentations are performed. Consequently, sixteen indentation tests are done on a molar with a given orientation. Two molars with the identical orientation are used to duplicate the indentation tests. Therefore, a total of sixty-four indentation tests are performed on the exposed surfaces of the four molars in this study.

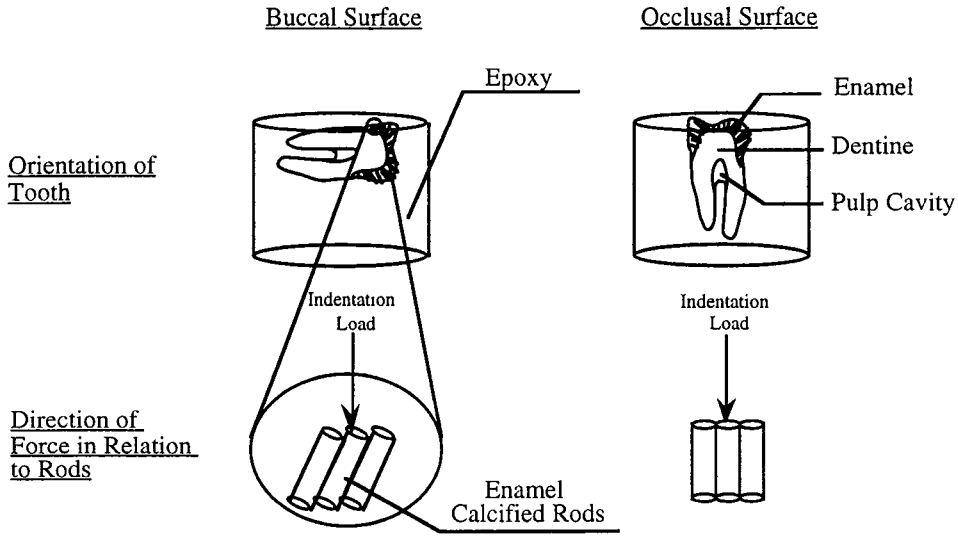

Figure 1. Specimen Preparation of the Human Teeth at Two Different Orientation of the Calcified Rods

Four surface impressions obtained from the identation tests performed are illustrated in Figure 2. Among the four impressions, two are taken on the occlusal surfaces and two on the buccal surfaces The loading conditions are 400g and 2000g, respecitvely. On each impression, two diagonals across the indentation are measured using an optical microscope with 100x magnification. The Vicker's hardness number is obtained by dividing the applied load in kilograms force by the square of the measured diagonal mean in square millimeters, as seen in the following equation [10],

$$VHN = \frac{1.854 \cdot P}{d^2} \quad [\text{kg/mm}^2] \qquad (1)$$

where: P = load, in kgf, and d = mean diagonal of indentation, in mm. Table 1 lists the mean and standard deviation of the hardness measurements.

To analyze the results obtained from the hardness measurements, the two curves illustrated in Figure 3 are constructed using the data listed in Table 1. The solid line represents the mean hardness values measured on the occlusal surface and the dashed line the mean hardness values measured on the buccal surface as the loading condition varies from the low to the high. It is evident that the measured hardness of the human enamel

material, either on the buccal surface or on the occlusal surface, is a function of the loading condition. Examining the two plotted curves, a big hardness will be measured under a low

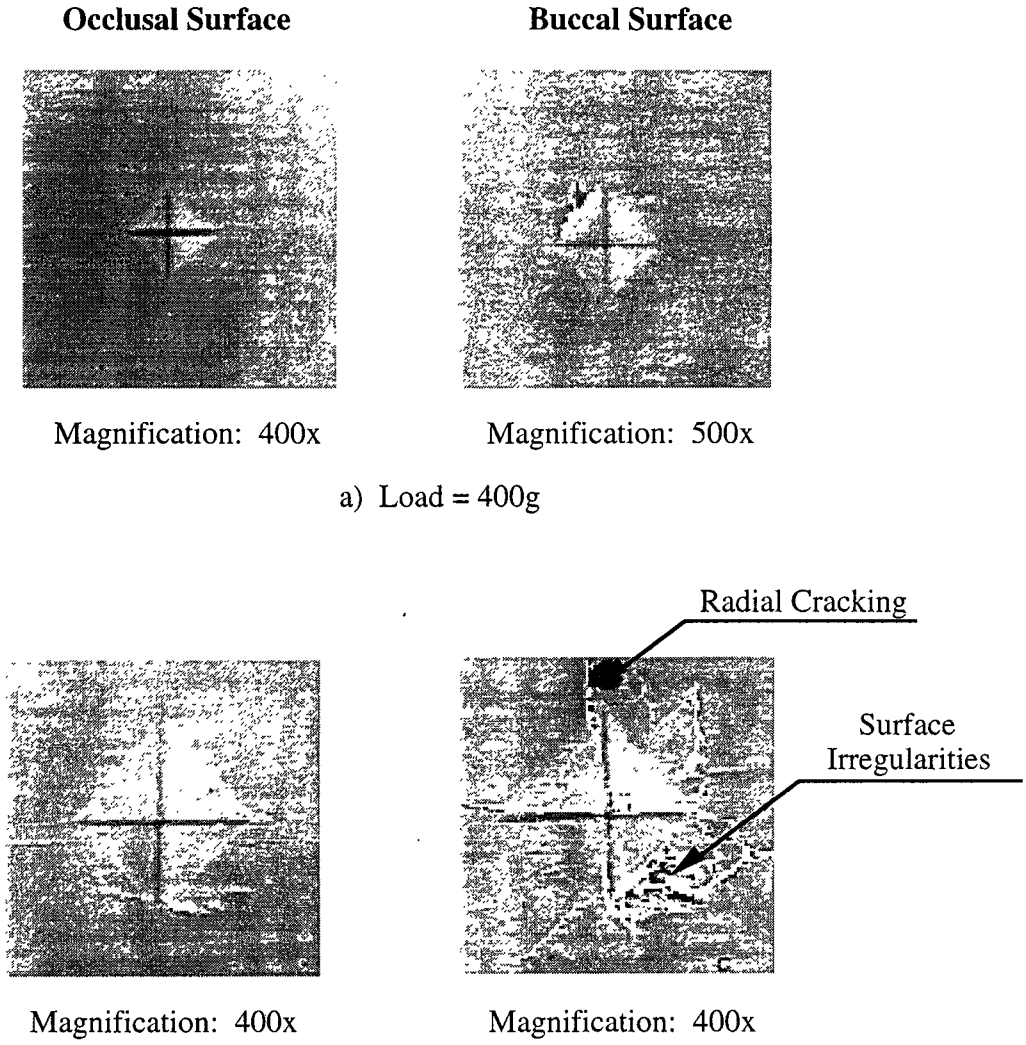

Figure 2. ESEM Micrographs of Indentations on the Occlusal and Buccal Surface at Loads of 400g and 2000g.

loading condition, and a small value of hardness under a heavy loading condition. The variation range covers from 380 VHN [kg/mm^2] when subjected to 400 grams force to 480 VHN [kg/mm^2] when subjected to 50 grams force. Important findings from analyzing the results obtained from the hardness measurements are as follows:

(1) Both curves follow the same trend, i.e., the measured hardness value declines exponentially as the loading increases.

Table 1. Data Obtained from Hardness Measurements

Vickers Hardness Number [Kg/mm^2]				
	Occlusal Surface		Buccal Surface	
Load (g)	Hardness Average	Standard Deviation	Hardness Average	Standard Deviation
50	468	6.6	453	14.5
100	453	13.3	426	23.2
200	430	17.4	412	18.8
400	398	18.3	390	36.3
800	395	3.2	383	8. 9
1000	381	7.4	351	37.2
2000	379	2.4	328	14.4

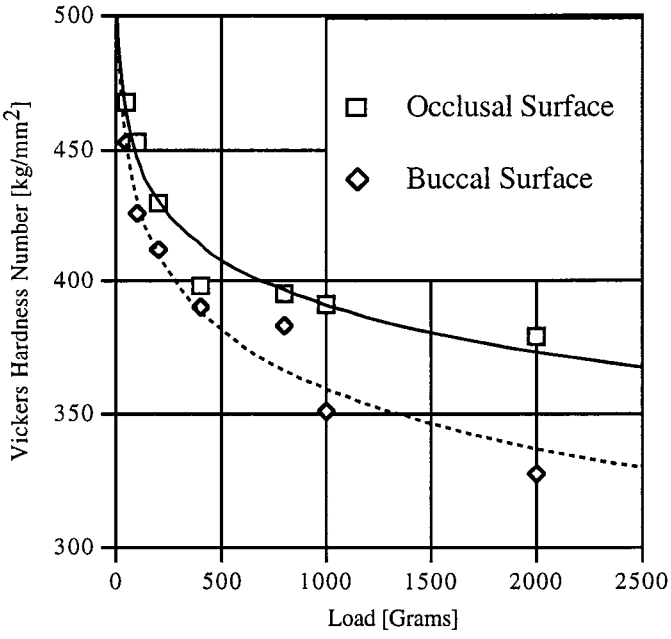

Figure 3. Hardness Curves of Enamel on Occlusal and Buccal Surface

(2) The occlusal hardness-load curve is consistently higher than the buccal hardness-load curve, indicating that the occlusal surface possesses stronger resistance to the indentation force than the buccal surface does.

(3) Standard deviations of hardness measurements on the buccal surface is between 8.9 to 37.2 VHN, which is significantly larger than the standard deviation range of 1.8 to 18.3 VHN observed on the occlusal surfaces. By examining the impressions shown in Figure 2, the large standard deviation is mainly contributed by the presence of a crack system developed during indentation.

3. Three-Dimensional Topography Analysis

The results from the hardness tests indicate that hardness of human enamel varies as the loading condition changes. In addition, the surface orientation has an effect on the hardness measurement. To gain a better understanding, further study is needed to interpret these observations and identify the significance of this material property on its clinical performance. Such information is important not only to the medical community, but also to the engineering community, which is responsible for designing and manufacturing the material to be used for dental restoration fabrication.

In this study, we apply a new methodology called three-dimensional topography analysis. Through visualization of the hardness impressions, characterization of their geometric shapes is performed using methods of image processing and atomic force measurements. Figure 4 illustrates the developed computer-based system to carry out the characterization. The main examination procedure is outlined as follows:

(1) Examination using scanning electron microscopy (SEM) to verify the hardness measurements;

(2) Examination using atomic force measurements (AFM) to obtain digitized indentation topography;

(3) Three dimensional visualization or reconstruction of indentations; and

(4) Quantitative characterization.

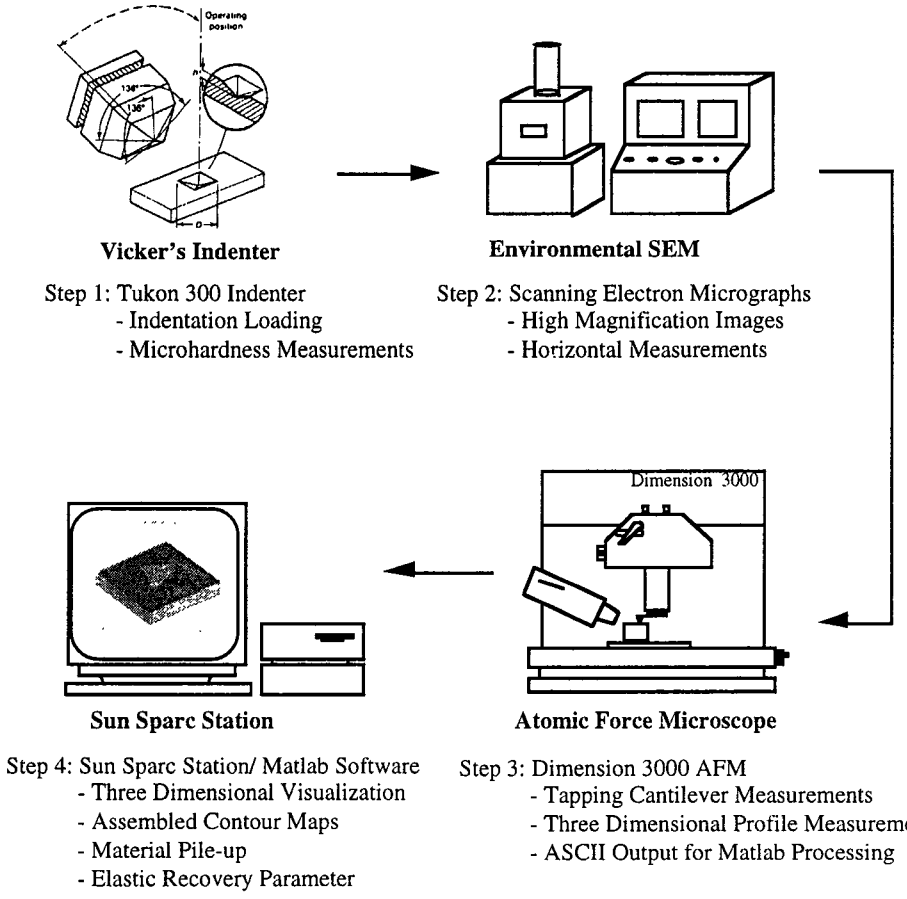

Figure 4. Computer-Based System for Characterization of Microhardness Indentations

3.1 SEM Examination

In this study, an Environmental Scanning Electron Microscope(ESEM) is used [11]. The four surface impressions illustrated in Figure 2 are SEM micrographs taken on both the occlusal and the buccal surfaces indented with loads of 400g and 2000g. The SEM micrographs allow accurate horizontal dimensional measurements to be carried out for verifying the micro-hardness measurements. These micrographs also provide a qualitative assessment of indentations, especially for the effect of the enamel rod structural system on the variations in hardness measurements and fracture patterns formed during indentation.

Examining the four micrographs shown in Figure 2, two important observations can be made. The first observation is that the illustrated geometric shape on the occlusal

surface reflects the geometry of the indenter. Therefore, the impression has a well defined geometry. Note the rod orientation on the occlusal surface. Because rods primarily extend perperdicularly from the dentinoenamel junction and are generally perpendicular to the occlusal surface. During indentation, the rods are parallel to the applied force through the Vicker's indentor and are subjected mainly to compression. Under the compression stress field, the impression is formed under the built-up hydro-static pressure. The indentations at both loading conditions, 400g and 2000g, give a geometrical shape that matches the geometry of the Vicker's indentor. As shown in Figure 2, radial cracks on the occlusal surface can be observed emanating from corners of the surface impression, at heavy loads, suggesting the release of the accumulated strain energy from the rods. The strain energy is dissipated through plastic deformation and in the process of forming a crack system.

The second observation is that as the load increases, the extent of the resulting damage on the crack pattern formed on the indentation becomes more severe. As illustrated in Figure 2, surface deformation and surface irregularities increase with increasing loads from 400 g to 2000 g. On the occlussal surface, the size of the radial cracks increases with increasing load. The crack pattern remains the similar as that of lower loads. Comparable conclusions can be drawn for the buccal surface. As previously mentioned, both radial cracking and surface irregularities can be found on the buccal surface indentations. It is obvious that the extent of the development of these two types of damage increases dramatically from the 400g to 2000g.

3.2 Atomic Force Microscopy

Elastic recovery at hardness indentatioons is a phenomenon well recognized by the research community. As illustrated in Fiugre 5, the identation process starts in loading, then elastic deformation, plastic deformation, unloading, recovery of the elastic deformation and finally the residual surface impression.

Studies of impression geometries in metallic and non-metallic materials using various standard microhardness indenters indicate that whereas characteristic in-surface dimensions generally remains a resonable measure of those at maximum loading, (thereby justfying a definition of hardness in terms of post-indentation measurements), the depth of the impression does not. Extremes in depth recovery are shown by 'soft' metals, where it is negligible, and 'highly elastic' rubbers, where it is nearly complete. Therefore, the phenomenon of elastic recovery is an important indicator characterizing the material

property to resist the irreversible deformation. Unfortunately, most of the formulas used for hardness evaluation, such as the formula presented in equation 1, do not count the factor of elastic recovery. As a result, an accurate assessment of material hardness is, if not impossible, difficult to achieve. This is especially true in evaluating the hardness of brittle solids where elastic recovery is usually significant. Another phenomenon to characterize the irreversable, or plastic, deformation is so-called 'pile-up' and 'sink-in', as illustrated in Figure 8. These surface disturbances are formed by dislocation loops generated under shear stress. It is evident that an accurate assessment of hardness has to incorporate both elastic and plastic deformations into the evaluation. To quantify these phenomena, the traditional SEM method is not adequate. A new approach, which is capable of performing measurements in the three-dimensional space, is needed.

In this study, a Dimension™ 3000 Atomic Force Scanning Probe Microscope is used to capture the topographic heights of the indentation geometry in micro-scale [11-13]. The indentation topographic data are obtained using a sampling area of 64 x 64 μm and

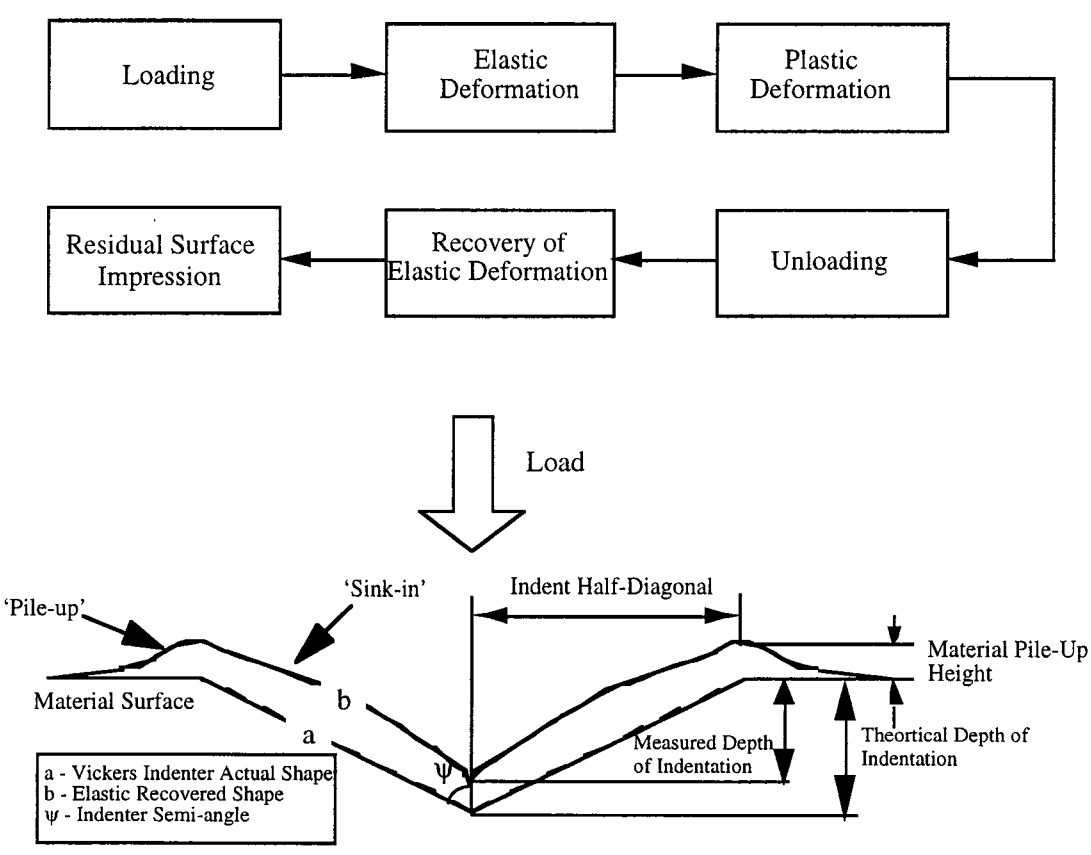

Figure 5. Identation Cycle and Illustration of the Profile of Indentation

represents an image resolution of 256 x 256 pixels in both x and y direction. The Z direction accuracy is 1 x 10^{-3} μm and has a maximum depth measurement capability of 6 μm. In processing the data, several software tools are used, including NIH IMAGE and MATLAB [14-15].

3.3 Three Dimensional Visualization of Indentation

3D image is reconstructed based on the Atomic Force Microscope measuments obtained from the indentations. Several aspects of the three-dimensional visualization of the indentation topography are presented in this section, as illustrated in Figure 6. They are (1) Isometric plot, (2) Contour map, and (3) Inverted isometric plot [16].

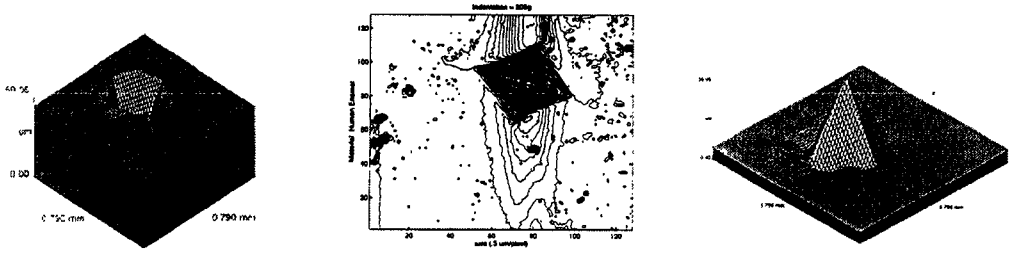

a) Isometric Plot b) Contour Plot c) Inverted Isometric Plot

Figure 6 Procedure of 3D Visualization using Image Processing

Figure 7a presents two 3D isometric plots of the indentations at 200g and 400g on the occlussal surface, respectively. The two 3D isometric plots shown in Figure 7b illustrate the same loading condition on the buccal surface. The basic topographic features of the indentation, namely the 'pile-up', 'sink-in', and the shape of the diamond of the microhardness tester, are observed from these isometric plots. These features give a vivid picture of the deformation process during identation. In the occlusal case, the rods are perpendicular to the applied load and do not fracture. Thus, a high hardness value is obtained for the occlusal surface and a small amount of pile-up and sink-in volume is found for both indentations at 200g and 400g, as illustrated in Figure 7a. In the bicca; sirface. the applied force acts at an angle to the rods, thus causing them to fracture and displace in various directions. The broken and mis-aligned rods appear in Figure 7b at the signficant damage zone located on the edge of the impression, indicating possible shearing

among the enamel rods due to its angular orientation nature on the buccal surface with respect to the loading condition. In addition, plastic flow of material forms 'pile-ups' and 'sink-ins'. The volume of these surface disturbances, as observed from Figure 7b, is relatively large if compared with the occlusal case.

Figures 8a and 8b present two contour plots taken from the three dimensional indentation topographies as displayed in Figure 7. A total of forty equally-distant contour levels based on the total height of each indentation topography is used. The significant advantage of the contour plot of impression is that it provides information of a directional nature relating to the surface topography. It's important to notice the asymmetry of the indentation on both the occlusal and buccal surface. The asymmetry is an imprint of the inhomogenous response of the enamel rods matrix to the indentation loading. It suggests the disturbance produced in enamel is irregular. In Figure 8a, the asymmetry of the indentation on the occlusal surface is conformed to two main islands of pile-ups on two sides of the indentation. In Figure 8b, the asymmetry of the indentation on the buccal surface is more severe, as both fracture and deformation specifically developed on one side of the indentation impression.

In order to see the topographic details of the part of impression below the general level of the surface, two inverted isometric plots of the indentations on both occlusal and buccal surface are presented in Figure 9. These inverted plots exhibit the plastic deformation of the material. The pile-up is seen from the surrounding edges of the indentation. Just above the level of the surface, there is evidence of small amounts of sink-in before the shape of the indentation follows exactly the shape of the diamond indentor. From Figure 9a, a small amount of the sink-in volume of the impression is found on the occlusal surface. From Figure 10b, a much greater amount of the sink-in volume is revealed immediately above the edges of the indentation. It is interesting to note that a significant amount of fracture can be observed on one side of the indentation at 400g loading. This phenomenon can also be confirmed if the correponsing contour plot is examined. This fracture region could be due to the shearing of enamel rods during the indentation unloading cycle. Overall, the qualitative assessment of the indentation morphology using the atomic force microscope can be summarize in the Table 2.

Table 2. Summary of 3D Visualization Results

	Major Observations		
	Isometric Plot	Contour Plot	Inverted Isometric Plot
Usage	Visualization of basic properties, e.g., pile-up, sink-in, and the shape of impression indenter	Provides information of a directiona nature relating to the surface topography	Exhibit the plastic deformation of thematerial below the level of the indentation impression
Occlusal Surface	1) Small amount of pile-up and sink-in volume is found for both indentations 2) The dominant mechanism is uniform plastic deformation of the material	1) The asymmetry of the indentation on the occlusal surface is conformed to two main islands of pile-ups on two sides of the indentation	1) A minimal amount of sink-in of the indentations is found on the occlusal surface
Buccal Surface	1) A large amount of pile-up volume is observed at one corner of the indent, indicating possible shearing of the enamel rods due to its angular orientation nature on the buccal surface	1) The asymmetry of the indentation on the buccal surface is more severe, as both fracture and deformation specifically developed on one side of the indent.	1) A much greater amount of sink-in is revealed immediately below the edges of the indentation. 2) A significant deformation zone is also found on one side of the indentation at 400g loading

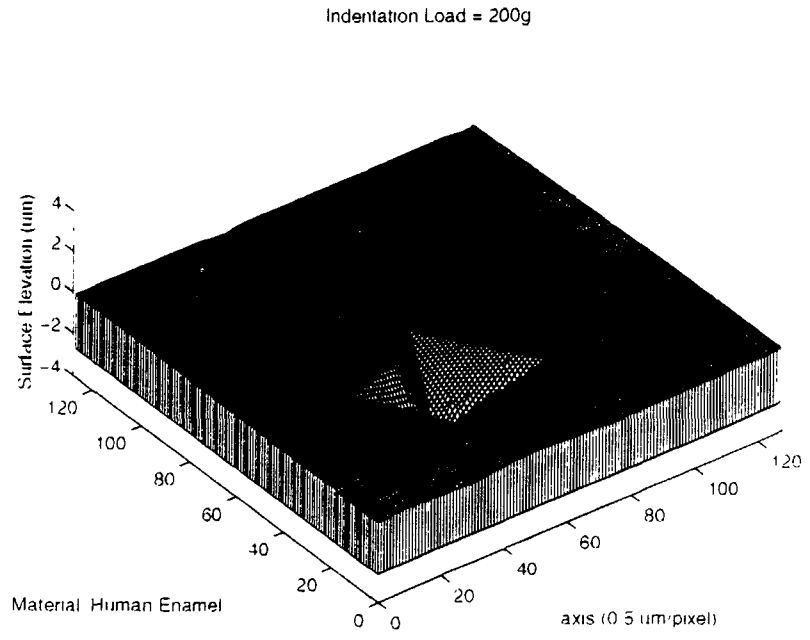

a) Indentation Load = 200 g

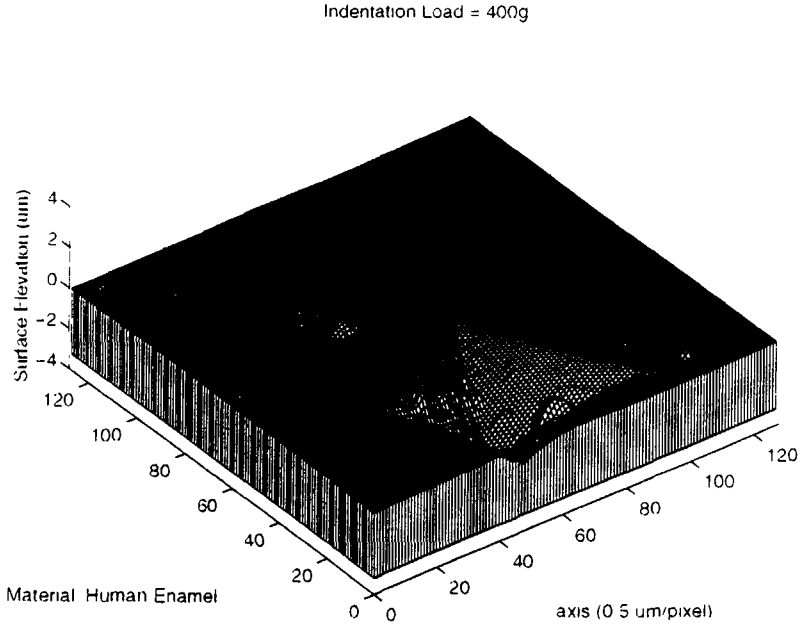

b) Indentation Load = 400 g

Fig. 7a. Three Dimensional Topography Visualization of the Indents on Occlusal Surface

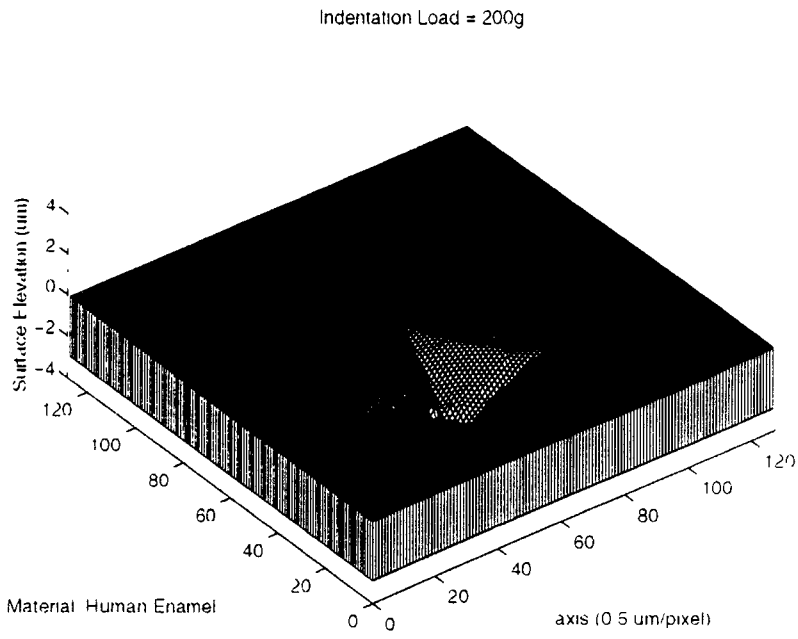

a) Indentation Load = 200 g

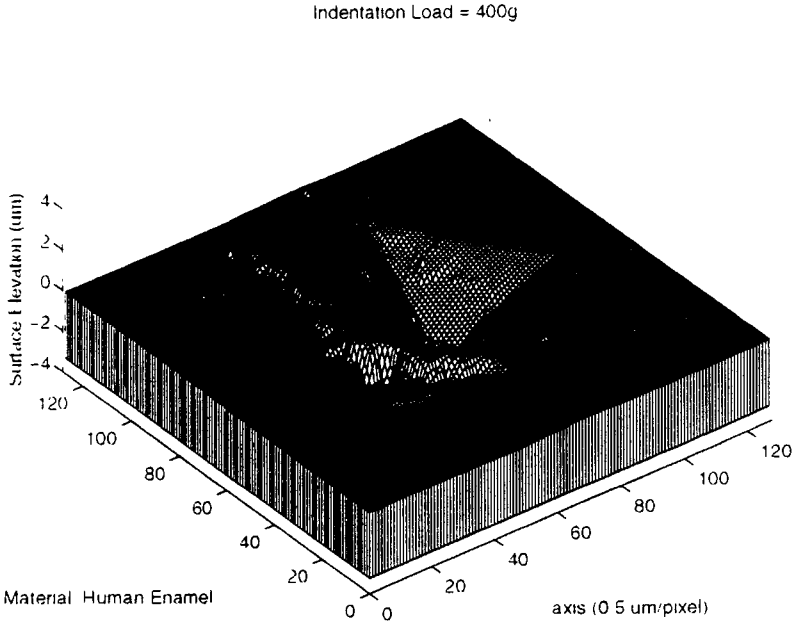

b) Indentation Load = 400 g

Fig. 7b. Three Dimensional Topography Visualization of the Indents on Buccal Surface

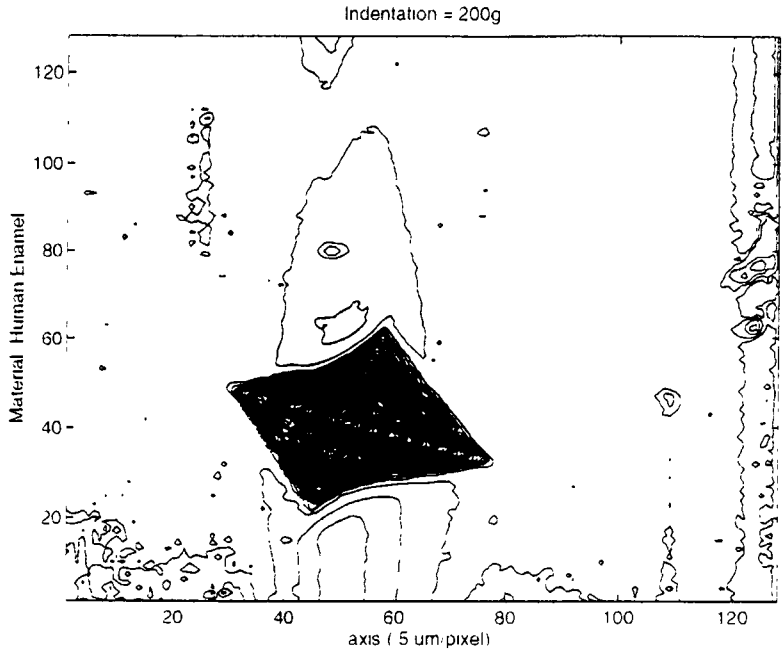

a) Indentation Load = 200 g

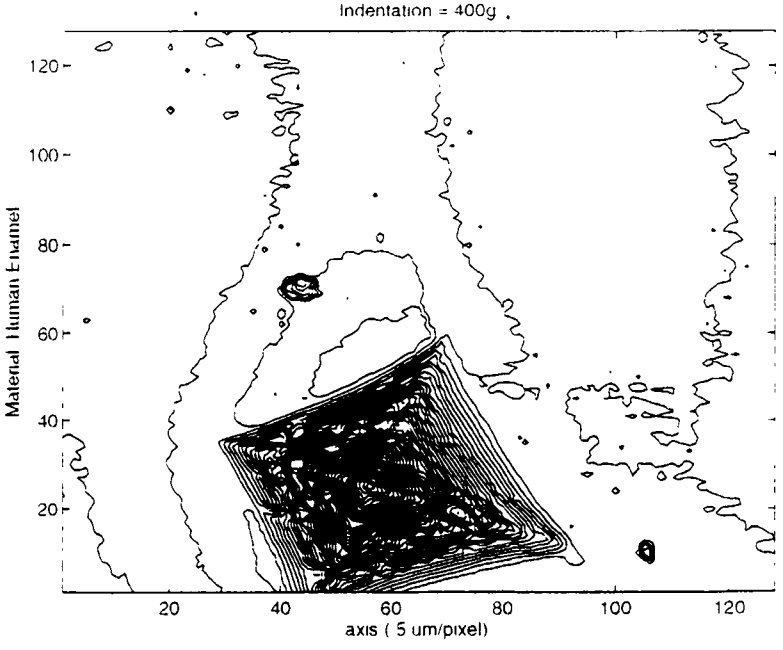

b) Indentation Load = 400 g

Fig. 8a. Contour plots of microhardness indentations on occlusal surface

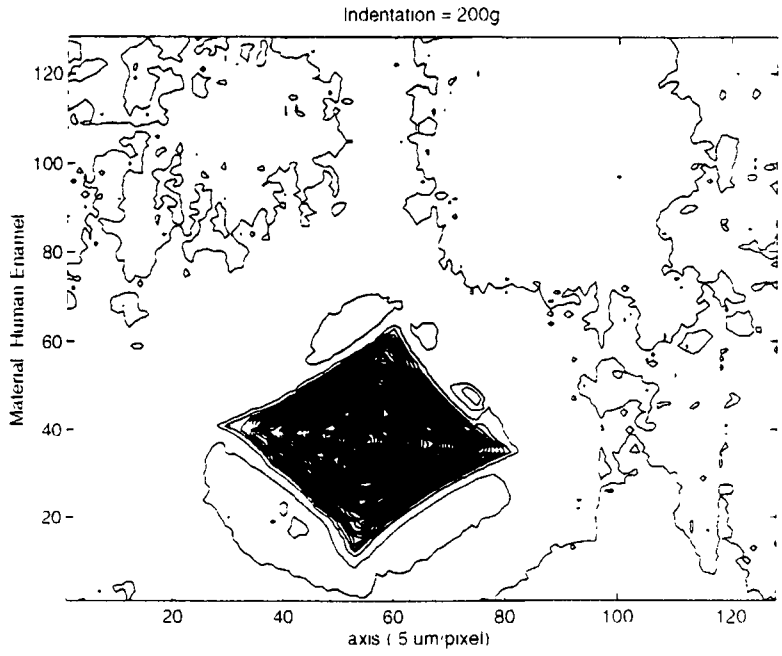

a) Indentation Load = 200 g

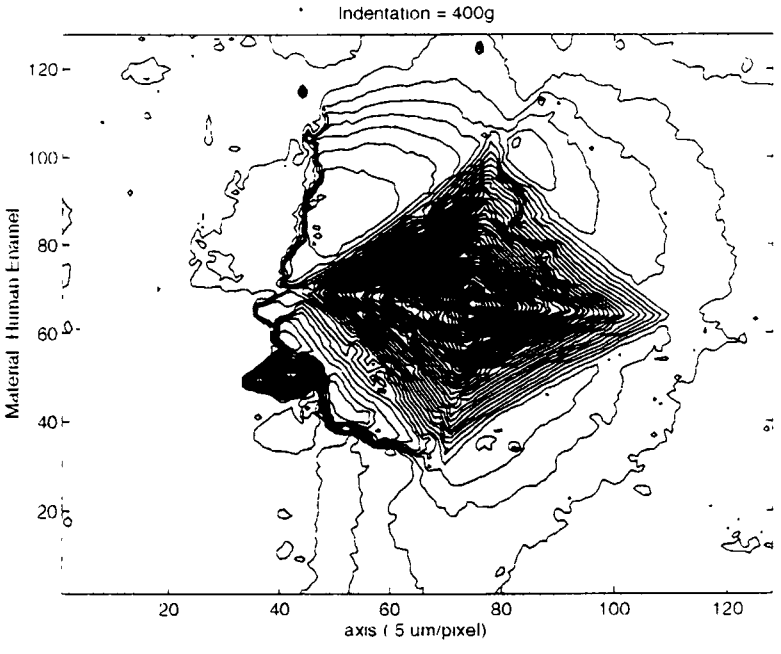

b) Indentation Load = 400 g

Fig. 8b. Contour plots of microhardness indentations on buccal surface

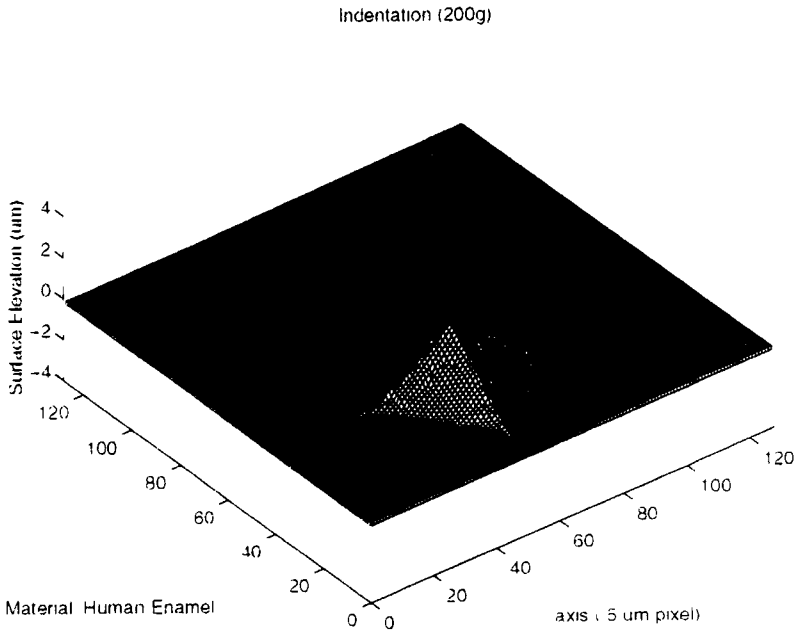

a) Indentation Load = 200 g

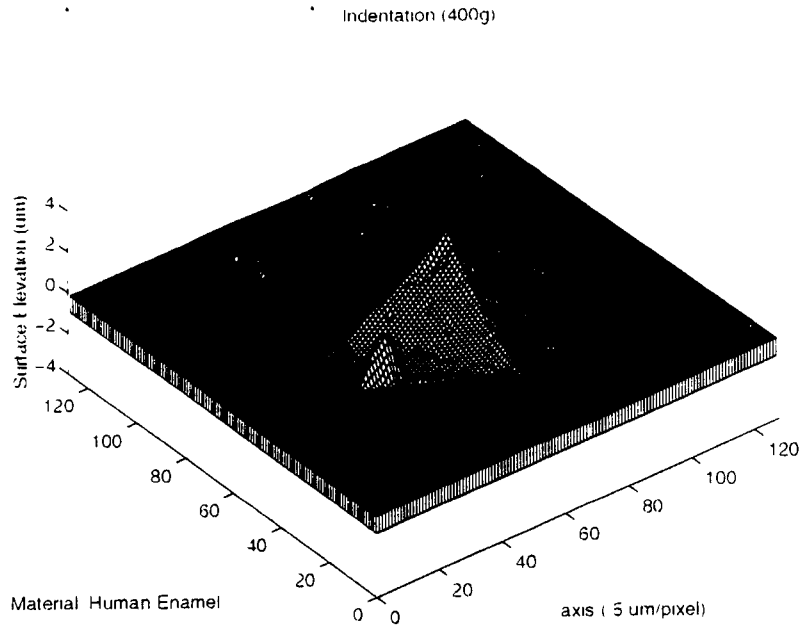

b) Indentation Load = 400 g

Fig. 9b. Inversion plots of microhardness indentations on buccal surface

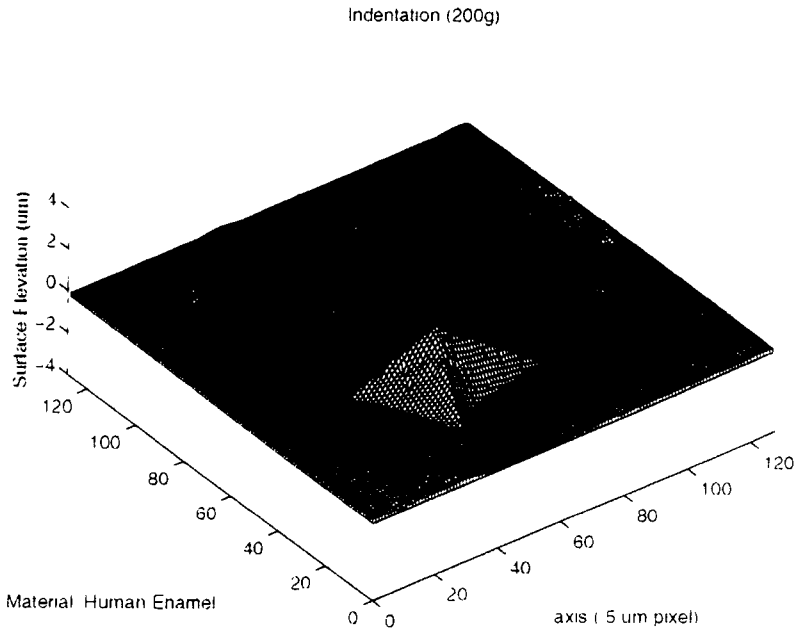

a) Indentation Load = 200 g

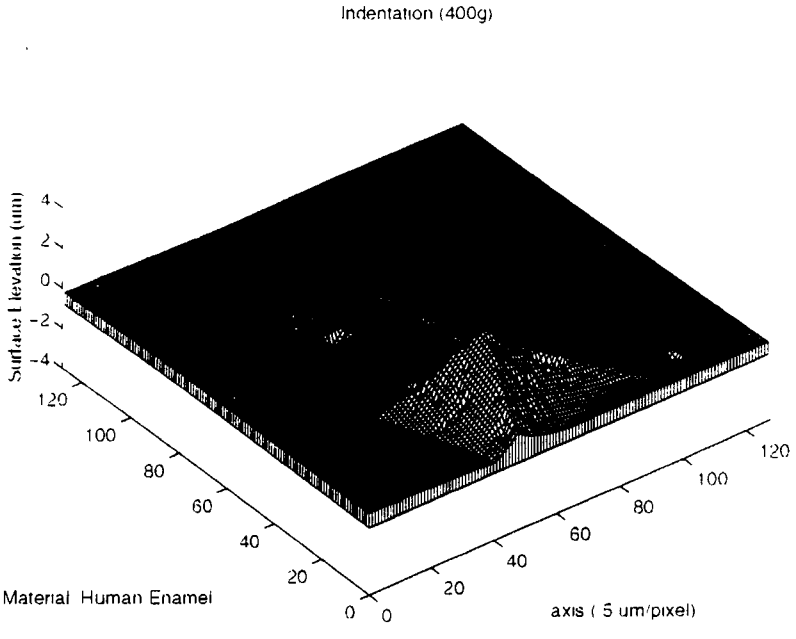

b) Indentation Load = 400 g

Fig. 9a. Inversion plots of microhardness indentations on occlusal surface

4. Discussion of Results

Information gained from the 3D visualization offers great opportunities to understand the physical process of hardness identation. The digitized data obtained from the atomic force microscopy measurements form a basis to perform quantification of the hardness identiation process. The three aspects discussed in this paper are elastic recovery of the indentation impresssion in brittle material, characterization of plastic flow, and normalization of hardness measurements with respect to a selected loading condition.

4.1 Elastic Recovery in Brittle Material

To quantify elastic recovery at hardness indentations, a new parameter is defined as follows:

$$\textit{Elastic Recovered Index} = \frac{\textit{Predicted Depth} - \textit{Measured Depth}}{\textit{Predicted Depth}} * 100\% \qquad (2)$$

In this study, the elastic recovery is calculated as a ratio of the difference between the predicted and measured depths to the predicted depth. It is expressed as a percentage. Note that an assumption is made in this study to calculate the predicted depth. It is assumed that the dimension of indentation diagonal remains unchanged during the elastic recovery process. Based on the assumption, the predicted depth is given by

$$\text{Predicted Depth} = (\text{Indent Half Diagonal}) * \cot\psi \qquad (3)$$

where parameter ψ represents the semi-angle of the indenter. It is equal to 74.05^{o} in this study. It should note that the measured depth can be readily obtained by sorting the data in the depth direction and identifying the most negative number with respect to the reference planary surface, i.e.,

$$\text{Measured Depth} = \max \sum \text{abs}(\text{depth}_i) \qquad (4)$$

Table 3 lists numerical values of the elastic recovery of hardness indentations. Data used for calculation are taken from the atomic force microscopy measurements for the two loading conditions of 200g and 400g for both occlusal and buccal surfaces.

Table 3. Results of the Indentation Height Parameters

	Occlusal Surface		Buccal Surface	
Load (g)	200g	400g	200g	400g
Measured Depth of Indentation(μm)	2.59μm	3.20μm	2.86μm	3.24μm
Theoretical Depth of Indentation(μm)	4.21μm	6.23μm	4.21μm	6.23μm
Elastic Recovered Index (%)	37%	49%	32%	48%

Examining the listed data, two important observations can be made. The first observation is that elastic recovery along the depth direction is significant at low loading conditions, such as 37% at 200g versus 49% at 400g for the occlusal surface. In fact this is true for both occlusal and buccal surfaces. The second observation is that the elastic recovery is more significant with the occlusal surface than the elastic recovery with the buccal surface, such as 37% versus 32% at 200g, and 49% versus 48% at 400g. However, such differencs decrease as the loading condition increases. This is due to the presence of a dominant crack system usually formed under high loading conditions.

4.2 Characterization of Material Plastic Flow

Material plastic flow can be characterized by the 'pile-ups' and 'sink-ins' formed during the indentation process. In this study, a parameter, denoted as pile-up height index, is introduced to characterize the formed 'pile-ups'. It is given by

$$\text{Pile - Up Height Index} = \frac{\text{Mean of the heights of pile - ups}}{\text{Predicted Depth of Indentation}} * 100\% = \frac{\frac{1}{n}\sum_{i=1}^{n} h_i}{\text{Predicted Depth of Indentation}} * 100\% \quad (5)$$

Table 4 lists numerical values of the pile-up height index for the hardness indentations used in section 4.1. It is interesting to note that numerical values of the pile-up height index are relatively low, 3.5% at 200g and 3.6% at 400g, for the occlusal surface.

On the other hand, numerical values are relative high, 12.4% at 200g and 14.3% at 400g, for the buccal surface. This difference points out the effect of rod orientation with respect to the loading surface on the material plastic flow during indentation.

Table 4. Pile-up Height Index

	Occlusal Surface		**Buccal Surface**	
Load (g)	200g	400g	200g	400g
Mean Pile-up Height (μm)	0.15μm	0.23μm	0.52μm	0.89μm
Predicted Depth of Indentation(μm)	4.21μm	6.23μm	4.21μm	6.23μm
Pile-up Height Index (%)	3.5 %	3.6 %	12.4%	14.3%

In order to graphically characterize the material flow during indentation, a second parameter, called spread area index, is introduced. The parameter is defined by

$$[\text{Spread Area Index}]_i = \frac{\sum_x \sum_y \text{Solid Area within a Sliced x - y plane}}{\sum_x \sum_y \text{Total Area within a Sliced x - y plane}} \qquad (6)$$

for i = 1, 2, 3, ... N where N represents the number of slices taken along the z- direction. Note the solid area is determined by the materialized area which results in the intersection of a sliced horizontal plane and the indentation impression. Table 5 lists numerical values of the spread area index on 10 sliced x-y planes.

Table 5. Numerical Values of Spread Area Index

	Spread Area Ratio [%]									
Z-Direction Height (μm)	0.4	0.2	0	-0.2	-0.4	-0.8	-1.2	-1.8	-2.2	-2.6
Occlusal Surface (200g)	0.1%	0.3%	90.3%	93.9%	94.9%	96.7%	97.9%	99.2%	99.7%	99.9%
Buccal Surface (200g)	4.6%	9.4%	93.8%	94.8%	95.7%	97.2%	98.3%	99.4%	99.8%	99.9%
Occlusal Surface (400g)	.13%	0.9%	88.1%	90.1%	91.6%	94.4%	96.4%	98.2%	99.0%	99.6%
Buccal Surface (400g)	5.9%	14.7%	85.5%	90.2%	91.8%	94.3%	96.3%	98.3%	99.2%	99.7%

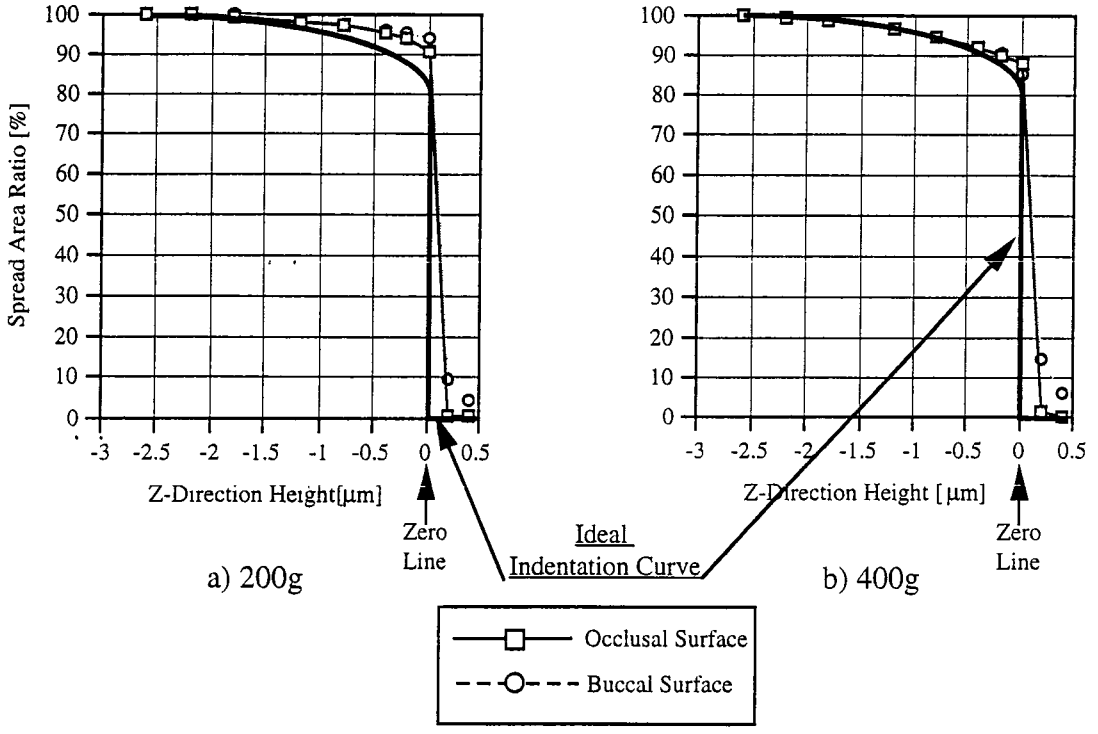

Figure 10. Graphical Illustration of Material Flow during Indentation

Figure 10 presents two plots of the listed data. Note the curve in dark line, which represents an ideal indentation process without any 'pile-ups' and 'sink-ins'. The top part of the ideal curve has a slope, which characterizes the increase of indented area. The sudden drop portion indicates the sliced x-y plane is just passing the reference surface, on which 'pile-ups' are built in. The zero line is the characteristic of no any 'pile-ups' formed during indentation. Therefore, any deviation from the ideal curve is indication of material plastic flow. The deviation on the top portion represents 'sink-ins'. The deviation on the

bottom portion characterizes 'pile-ups'. The closed area between the ideal curve and the measured curve represents the volume of materal plastic flow, i.e.,

$$\text{Plastic Flow Volume} = \int_{z=0}^{\text{max pile-up height}} [g(z) - f(z)]\, dz \qquad (7)$$

The two curves in Figure 10a represent the spread area index curved based on the calculations for both the occlusal and buccal surface at 200g. The two curves in Figure 10b represent a similar situation except the loading condition is at 400g. All the four curves indicate that 'sink-ins' are much less significant than 'pile-ups' in the determination of plastic flow volume because the deviation on the top portion seems negligible if comparing it with the deviation on the bottun portion. Examining the two curves in either Figure 11a or Figure 11b, the total deviation for the occlusal surface is always less than that for the buccal surface. There are more 'pile-ups' formed, or more plastic flow, on the buccal surface than those formed on the occlusal surface. The materal plastic flow volumes for the four cases are calculated using the integration formula, equation 7, are listed as.

Rod orientation:	Occlusal Surface		Buccal Surface	
Loading:	200 g	400 g	200 g	400 g
Plastic flow volume: [unit: 10^3 μm]	78	208	135	253

4.3 Normalization of Hardness Measurements

The hardness values measured under different loading conditions differ from each other significantly. As shown in the data listed in Table 1, the maximum number is 468 VHN at 50g and the minimum number 379 at 2000g for the occlusal surface. Therefore, telling a hardness number without giving the corresponding loading condition may not provide sufficient information on the hardness property of the material. Normalization of the hardness measurements made under different loading conditions with respect to a selected, or commonly acceptable, loading conditioon is needed.

If examining the formula used to determine the hardness value from measurement, such as equation 1, a surprising fact is that the geometrical parameter used is the dimension of the impression diagonal. This parameter has the least effectiveness in characterizing the reversible deformation occurred during indentation. The credibility of determining hardness value without taking to account the reversible deformation, such as elastic recovery of the indentation depth, is in question.

In this study, a procedure to perform normalization and incorporate the reversible deformation into the hardness determination is proposed. Equation 1 is revised and two new parameters are introduced.

$$\text{Normalized Hardness} = \frac{1854 * P}{d^2} * \sqrt[4]{\text{Elastic Recovered Index}} * C \qquad (8)$$

The first parameter is based on the elastis recovery index. Recognizing the non-linearity between the material hardness and elastic recovery, a fourth root is used. As an example to demonstrate the introduction of this parameter, the following data are before and after the normalization for the occlusal surface together with the four numerical values of elastic recovery index:

$$\text{Normalized Hardness} = \frac{1854 * P}{d^2} * \sqrt[4]{\text{Elastic Recovered Index}} \qquad (9)$$

before normalization:	468	453	430	398
elastic recovery index	29%	25%	37%	49%
after normalization:	328	331	334	326

As indicated, the normalized hardness values are 328, 331, 333, and 326, that are very close to each other and vary slightly about 330 HVN. Numerical values of these four normalized hardness measurements may not seem reasonable if comparing their values measured before normalization. These values are 468, 453, 430, and 398, respectively. Therefore, there is a need to make an adjustment for the normalized hardness value be set at a given loading condition. Say the loading condition of 200g is slected. The parameter C in equation 8 can be set at the following value:

$$C = \sqrt[4]{3} = 1.316 \tag{10}$$

Using this correction factor to adjust the normalized hardness values will allow us to raise the average of the normalized hardness values to a new level. It is now at 430 HVN because the four normalized hardness values after adjustment are 431, 435, 439, and 429 HVN, respectively, as illustrated in Figure 12. Graphically speaking, such a normalization and adjustment process is to bend a curve to a horizontal line and then shift the line upward or downward. In this study, the shift value is 100 VHN.

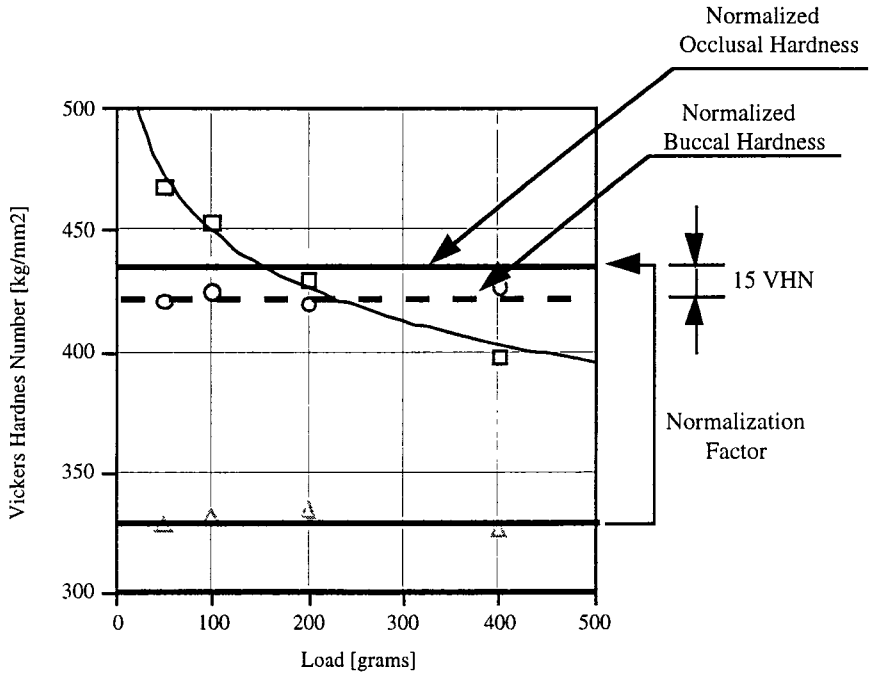

Figure 12. Illustration of Hardness Normailzation

The significance of implication of this normalization process is two-fold. First, the normalized hardness values are determined not only by the applied load and the measured diagonals of the impression, but also by incorporating the reversible deformation into the hardness evaluation. As a result, the normalized hardness value will have a unique hardness value for a given type of ceramic material without specifying the loading condition under which a specific indentation test is performed.

The second contribution of this normalization process is the establishment of a criterion to use the hardness measurement as a tool for comparison among different ceramic materials. In this study, we obtained two curves, one for the occlusal surface and the other for the buccal surface. Using equation 8 and having parameter C set at 1.316, the normalized hardness value for the occlusal surface is 435 VHN, and the normalized hardness for the buccal surface is 420 VHN. Therefore, comparison between the two normalized values clearly indicates that the hardness of the occlusal surface is higher than that of the buccal surface. The difference is about 6-10 %, mainly due to the orientation of rods with respect to the loading surface.

5. Conclusions

A research effort to perform a combined analytical and experimental study with focus on identifying crack fracture characteristics in microhardness indentation of human dental enamel. Significant findings are summarizes as follows.

1. Vickers Microhardness indentation using loading conditions, from 50g to 2000g has been performed on both occlusal and buccal surfaces in human enamel. Significant cracking fracture and deformation patterns have been observed.

2. A computer-based Scanning Electron Microscope and Atomic Force Measurement Analysis system has been used to perform surface height measurements of the indentation topography. These measurements are used to visualize hardness indentations using computer graphics software. Three types of visualization plots of the indentation have been presented, 1) isometric plot, 2) contour map, and 3) inverted isometric plot, providing a vivid picture and rich information into the material fracture and deformation druing the indentation process.

3. Quantitative indices, such as the pile-up height, material spread area, and pile-up volume have been introduced to serve as performance indices to evaluate the material property of human enamel material. Results from this study affirm that difference in enamel rod orientation contributes to variation of hardness characteristics and modify the cracking mechanism in an intrinsic way.

4. A new formula to determine microhardness values for identation tests is proposed in this research. By incorporting elastic recovery into evaluation, a normalized hardness measurement can be achieved to associate a given type of ceramic material with a unique hardness value. This approach offers a unique opportunity to use hardness measurement as a means for comparison and other investigations related to material hardness characteristics.

Acknowledgment

The authors acknowledge the support from the University Research Board, the Mechanical Engineering Department, and the Institute for Systems Research under NSFD CDR-88003012 grant and NIDR grant P01-DE01976. Special thanks are due to the Northeast Consortium for Engineering Education (NCEE) of the Department of Defense for their support of this work. The authors would also like to thank Dr. Brian Lawn for providing use of the Normarski Microscope. Finally, sincere appreciation is also due to Mr. Daniel Young for his tremendous effort in taking atomic force measurements of microhardness indentations.

References

1. Zhang, G. M., Ko, W. F. , and Ng, S. J., " Submerged Precision Machining of Ceramic Material", Proceedings of 1995 Joint ASME Applied Mechanics & Materials Conference, AMD-Vol. 208, pp. 65-79., 1994.

2. Zhang, G. M., Ng, S. J., & Le, D. T., " Characterization of Surface Cracking Formed during the Machining of Ceramic Material", Proceedings of 1995 ASME International Mechanical Engineering Congress and Exposition, MED-Vol., 2-1, pp. 415-429, 1995.

3. D. Rekow, Zhang G. M., Thompson, V. P., " Machining Ceramic Materials for Dental Restorations", Proceedings of International Conference on Machining of Advancd Materials, NIST Special Publication 847, 1993

4. D. Rekow, " Dental CAD/CAM Systems: What is the State of the Art?", Journal of the American Dental Association, Vol. 122, 43-48, 1991.

5. Boyde, A., "The Development of Enamel Structure," Proceedings of the Royal Society of Medicine, 60, pp. 923-929, 1967.

6. Boyde, A., and Fortieus, M., "Development, Structure and Function of Rhinoceros Enamel," Zoological Journal of the Linnean Society, 87, pp. 181-214, 1986.

7. Kraus, B., Jordan, R., and Abrams, L., *Dental Anatomy and Occlusion*, Waverly Press, Baltimore, Maryland, 1969.

8. Bhussey, B. R., and Biddy, B. G., "Surface Changes in Enamel," Journal of Dental Research, 36:409, 1957.

9. Caldwell, R. C., Muntz, M. L., Gilmore, R.W., and Pigman, W., "Microhardness studies of intact surface enamel," Journal of Dental Restoration, 36:732-738, 1992.

10. ASTM Standard Test Method for Microhardness of Materials, E 384-89.

11. Wei, B. and Komvopoulos, K., "Nanoscale Indentation Hardness and Wear Characterization of Hydrogenated Carbon Thin Films", Journal of Tribology, Vol 117, pp. 594-601, 1995.

12. Dimension 3000 Scanning Probe Microscope Instructional Manual, Digital Instruments, Inc., 1994.

13. Sarid, D., *Scanning Force Microscopy with Applications to Electric, Magnetic, and Atomic Forces*, Oxford University Press, New York, Oxford, 1991.

14. NIH Image Version 1.58: Image Processing and Visualization Software, National Institutes of Health, 1994.

15. MATLAB: High Performance Numerical Computation and Visualization Software, The MATHWORKS, Inc., 1992.

16. Stout, K. J., Three Dimensional Surface Topogrpahy, Penton Press, London, 1994.

17. Lawn, B. R., Howes V. R., "Elastic Recovery at Hardness Indentations", Journal of Material Science, pp.2745-2752, 1981.

18. Lawn B. R., Fracture of Brittle Solids, Cambridge University Press, Cambridge, 1993.